Structural Engineering and Mechanics, Vol. 25, No. 1 (2007) 1-20

DOI: http://dx.doi.org/10.12989/sem.2007.25.1.001

Characterization of the dynamic behavior of a linear guideway mechanism

Jyh-Cheng Chang† and James Shih-Shyn Wu‡

Institute of Mechanical Engineering, National Chung-Hsin Univeristy, 250, Kuo-Kuang Rd., Taichung, Taiwan 402, R.O.C.

Jui-Pin Hung‡†

Institute of Precision Machinery and Manufacturing Technology, National Chin-Yi Institute of Technology, 35, Lane.215, Sec. 1, Chung-Shan Rd., Taiping, 411, Taiwan, R.O.C.

(Received July 21, 2005, Accepted August 1, 2006)

Abstract. Dynamic behaviors of the contact surface between ball and raceway in a guideway mechanism vary with the applied loads and hence affect the mechanical responses of machine tools. The study aims to investigate the nonlinear characteristics of dynamic behaviors at the rolling contact interface in linear guideway mechanisms. Firstly, analytical method was introduced to understand the contact behaviors based on Hertz contact theory in a point-to-point way. Then, the finite element approach with a three-dimensional surface-to-surface contact model and appropriate contact stiffness was developed to study the dynamic characteristics of such linear guideways. Finally, experiments with modal test were conducted to verify the significance of both the analytical and the numerical results. Results told that the finite element approach may provide significant predictions. The study results also concluded that the current nonlinear models based on Hertz's contact theory may accurately describe the contact characteristic of a linear guideway mechanism. In the modal analysis, it was told that the natural frequencies vary a little with different loading conditions; however, the mode shapes are changed obviously with the magnitude of applied loads. Therefore, the stiffness of contact interface needs to be properly adjusted during simulation which may affect the dynamic characteristics of the machine tools.

Keywords: linear guide; Hertz theory; contact stiffness.

1. Introduction

Recently, the requirement of precision machine technology in the field of modern science and industry is appreciable. For purpose of achieving high-speed and precise positioning, it is necessary to fully understand the mechanical charcateristics of the driving mechanisms. The lower frictional force and higher performance than traditional linear slide rail, ball-type linear guideway is now most widely applied as a driving mechanism. In such systems, force transferred between carriage blocks

† PhD Candidate
‡ PhD, Professor, Corresponding author, E-mail: sswu@dragon.nchu.edu.tw
‡† PhD, Associate Professor

and guideway is performed via ball bearing. In the analysis of static and dynamic behaviors, a linear spring is generally used to simulate the behavior of contact between balls and carriage. However, from the viewpoint of Hertz's contact theory, the deformation at the contact point of raceway groove is highly nonlinear related to the contact loading applied to the balls. This characteristic may cause the contact stiffness of the balls within guidway to vary with the acting loads. In addition, when the carriage block of a linear guide system withstands moments, the deformation of ball groove of the carriage may affect the contact stiffness and dynamic behavior of the guideway structures. Therefore, the influence of moments upon the dynamic behavior of linear guideway is worthy for further investigation.

In the past, there were numerous applications with Hertz's contact theory, of which Lynagh (2000) and Hernot (2000) discussed respectively the vibration and stiffness matrix of ball bearings via nonlinear relationship of Hertz. In addition, Pimsarn and Kazerounian (2002) also put forward the theory of PISE (pseudo-interference stiffness estimation) based on Hertz's theory, which was used to estimate the stiffness of gears. Through the study of a ball-type linear guideway, (Ohta 1999) (Ohta and Hayashi 2000) derived the governing motion equations by Lagrange's approach and utilized finite element method to identify the dynamic behavior of the carriage of a linear guideway, and the mode shapes were characterized as the lower rolling, yawing, pitching, vertical, higher rolling vibration. In their studies, the contact status between rolling balls and raceway groove of carriage and rail was modeled as an one-dimensional point-to-point contact model and the ball was substituted by an axial spring. However, the contact configuration of a guideway is actually a type of surface contact module and hence can not be fully described by such a spring element.

The study was aimed to investigate the nonlinear contact characteristics at the rolling interface in linear guide mechanisms. The Hertz's contact theory was employed and the nonlinear characteristics of the contact interface between ball and raceway groove of the carriage and rail was described. Taking the normal stiffness and tangent stiffness of two-dimensional point-to-point contact into account, we firstly derive the governing equations and vibration frequency of the guideway system by Lagrange's approach. In order to simulate the ball-type linear guideway in a realistic way, a surface-to-surface contact mode associated with the interface element was introduced at the rolling interface of a guideway finite element model. The dynamic characteristics under different loading conditions were predicted by analytical approach and the finite element approach, respectively, for comparison. As a validation, experiments with modal tests were carried out on a linear guideway and the measured data were compared with the previous calculating results.

2. Contact characteristic at rolling interface

2.1 Contact stiffness

According to the Hertz's contact theory, there is a nonlinear relationship between the local deformation at the contact point and the applied load when two objects are tightly forced to each other. For a ball type linear guideway, the deformation of the groove will increase with the load applied on the balls and the contact stiffness of the interface rises. Such a variation in contact stiffness will affect the dynamic behavior to a different extent. Therefore, in order to obtain the correct dynamic characteristic of a guideway, the contact stiffness must be suitably defined. From Johnson (1985) and Goldsmith (1960), the Hertzian contact stiffness is defined as shown in Fig. 1,

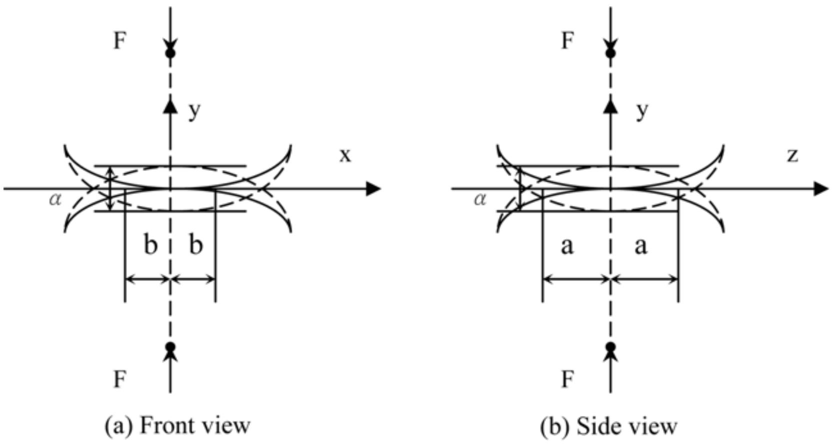

Fig. 1 Loadings and deformed shapes at contact boundary

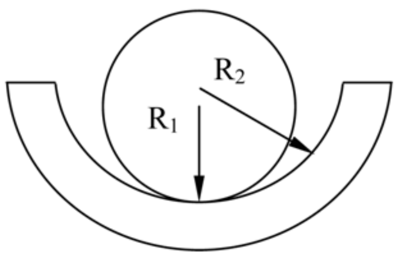

Fig. 2 Contact mode between sphere and cylindrical cup

where the relation between the deformation and the applied load are clearly described. In the figure, when a compression force F is applied, the contact boundary of two objects will deform a small amount of α with the contact area of ellipse shape. The relationships are given by the following formulas:

$$F = k_h \alpha^{3/2} \tag{1}$$

$$k_h = \frac{4}{3} \frac{q_k}{(\delta_1 + \delta_2)\sqrt{A + B}} \tag{2}$$

$$\delta_i = \frac{1 - \mu_i^2}{\pi E_i} \tag{3}$$

$$a = q_a \sqrt[3]{\frac{3F(\delta_1 + \delta_2)}{4(A + B)}} \tag{4}$$

$$b = q_b \sqrt[3]{\frac{3F(\delta_1 + \delta_2)}{4(A + B)}} \tag{5}$$

where α is the elastic deformation of the contact area, δ_i is the material properties of Hertz's contact theory, E is Young's modulus, μ is Poisson's ratio of material, a is the semi-major and b is the semi-minor of the contact ellipse. Constants A, B, q_a, q_b, and q_k were determined according to Goldsmith in 1960 where the contact configuration of a linear guideway can be simplified as a sphere with radius R_1 contacting to a cylindrical cup with radius R_2 (see Fig. 2), and

$$A = \frac{1}{2}\left(\frac{1}{R_1} - \frac{1}{R_2}\right) \tag{6}$$

$$B = \frac{1}{2R_1} \tag{7}$$

From Eq. (1), the normal stiffness can then be obtained as:

$$K_n = \frac{dF}{d\alpha} = \frac{3}{2}k_h\alpha^{(1/2)} \tag{8}$$

As was revealed in Hwang and Gahr (2003), the stiffnesses in normal and tangential direction are governed by the material properties of the bodies in contact, normal load, lubricant and surface roughness. In this study, the tangential stiffness K_S associated with frictional effect was therefore correlated with the normal stiffness K_n following the Columb's friction law.

3. The analytical method

3.1 The two-dimensional point-to-point contact model

The linear guideway analyzed in this paper is shown in Fig. 3 and the coordinate system describing the motion mode of the carriage is illustrated in Fig. 4, in which the origin of the *XYZ* coordinates is located at the mass center of the carriage and the x-axis is along the sliding direction of the carriage, β is the contact angle, d and e are the distances from the x-y plan and x-z plan to the contact point between the rolling ball and the carriage, respectively. Since the linear guide was designed with the contact geometry of an offset Gothic arc groove, a two point contact at the

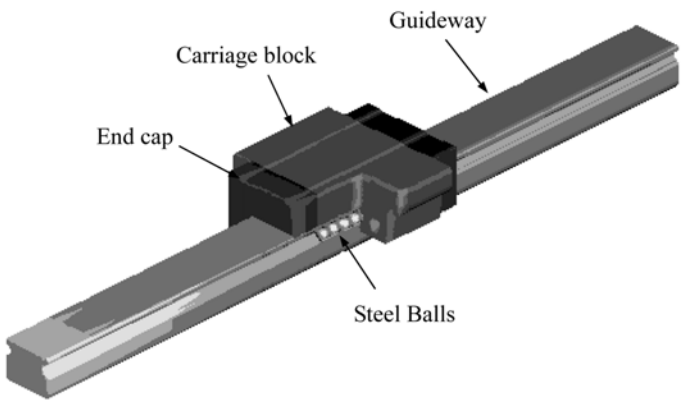

Fig. 3 Schematic of a linear guide system

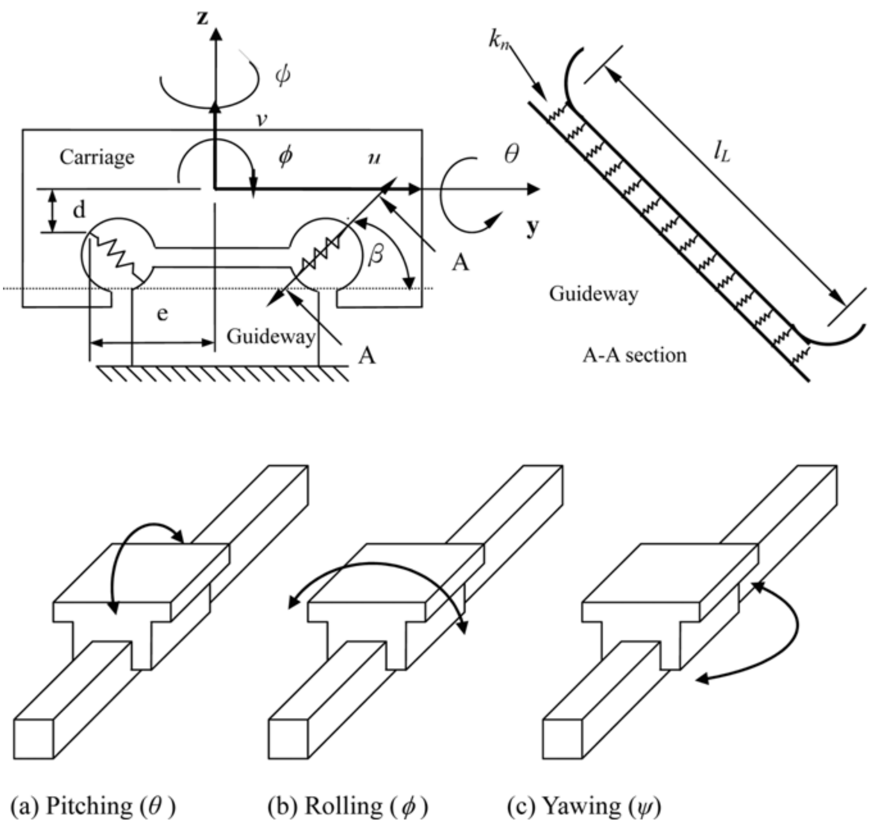

Fig. 4 Coordinate system describing the motion mode of carriage, in which β is the contact angle, u and v are the displacements in the y-axis and z-axis, respectively. ϕ, θ and y are the angular displacements about the x-axis, y-axis and z-axis, which are termed pitching, rolling and yawing motion, respectively (NSK Ltd.)

contact angle of 45 degree was formed between the balls and the carriage and the rail, respectively. To simplify such a two point contact mode, a series of spring elements with adequate spring constant are introduced at the raceway groove (Fig. 4). According to Ohta and Hayashi (2000), the spring constant per unit length of a distributed normal spring k_n in loading zone can be expressed as

$$k_n = \frac{Z_L K_n}{2 l_L} \tag{9}$$

where Z_L is the average number of balls running in the loading zone, l_L is the length of the loading zone and K_n is normal contact stiffness. It is worth noting that the term K_n in Eq. (9) is determined based on Hertzian theory, while the one used in Ohta and Hayashi (2000) is related to the vertical stiffness of the linear guideway, which is usually available in product menu provided by the manufacturer (NSK Ltd).

In addition, the contact force acting on the raceway groove of rail or carriage can be decomposed into positive normal force component and tangential force component. Therefore, it is understandable that the simulation of a point-to-point contact model with a spring element in contact normal direction can not fully describe the contact characteristics of the rolling interface and

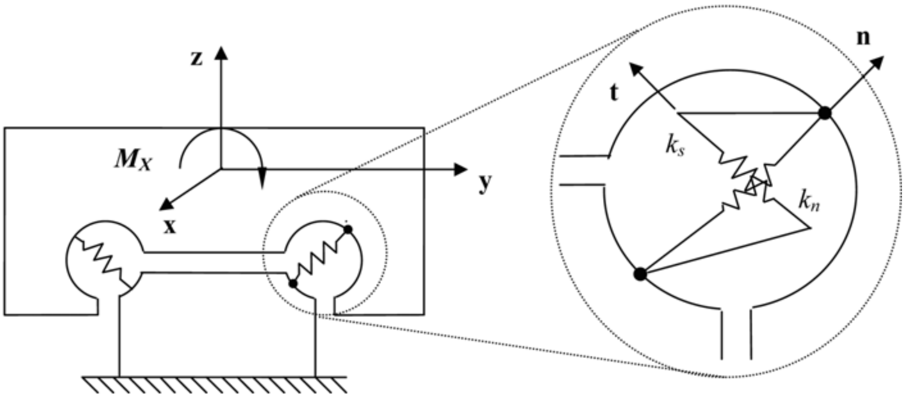

Fig. 5 Modeling of the rolling contact by using a spring element with normal stiffness k_n and another spring element with tangential stiffness k_s

another spring element with tangential stiffness was thus introduced in the tangential direction (see Fig. 4 and Fig. 5). The tangential stiffness k_S per unit length of the loading zone can finally be expressed as

$$k_s = \frac{Z_L K_s}{2 l_L} \tag{10}$$

3.2 Natural frequency of a linear guideway with rigid-body carriage

Here, for purpose of deriving the governing motion equation of the linear guideway system, the guidway and carriage are considered as rigid bodies and connected with a series of spring elements at the raceway groove. The kinetic energy E_K of the system in motion is given by

$$E_K = \frac{1}{2}M\dot{u}^2 + \frac{1}{2}M\dot{v}^2 + \frac{1}{2}J_x\dot{\phi}^2 + \frac{1}{2}J_y\dot{\theta}^2 + \frac{1}{2}J_z\dot{\psi}^2 \tag{11}$$

where M is the mass of carriage, J_x, J_y and J_z are the moment of inertia about the x-axis, y-axis and z-axis, respectively. $\dot{u}$ and $\dot{v}$ are the velocities along the y-axis and z-axis, respectively. $\dot{\phi}$, $\dot{\theta}$ and $\dot{\psi}$ are the angular velocity about the x-axis, y-axis and z-axis, respectively.

Since the carriage is supported by distributed normal springs and tangential springs, the potential energy E_p can then be given by

$$E_P = E_{P1} + E_{P2} \tag{12}$$

$$\begin{aligned} E_{P1} = \frac{1}{2}k_n\int_0^{l_L/2} [& \{(u - d\phi + l\psi)\cos\beta + (-v - e\phi + l\theta)\sin\beta\}^2 \\ & + \{(u - d\phi - l\psi)\cos\beta + (-v - e\phi - l\theta)\sin\beta\}^2 \\ & + \{(-u + d\phi - l\psi)\cos\beta + (-v + e\phi + l\theta)\sin\beta\}^2 \\ & + \{(-u + d\phi + l\psi)\cos\beta + (-v + e\phi - l\theta)\sin\beta\}^2]dl \end{aligned} \tag{13}$$

$$
\begin{aligned}
E_{P2} = \frac{1}{2}k_s\int_0^{l_L/2}[&\{(u-d\phi+l\psi)\sin\beta+(v+e\phi-l\theta)\cos\beta\}^2\\
&+\{(u-d\phi-l\psi)\sin\beta+(v+e\phi+l\theta)\cos\beta\}^2\\
&+\{(u-d\phi+l\psi)\sin\beta+(-v+e\phi+l\theta)\cos\beta\}^2\\
&+\{(u-d\phi-l\psi)\sin\beta+(-v+e\phi-l\theta)\cos\beta\}^2]dl
\end{aligned} \tag{14}
$$

where E_{P1} and E_{P2} are the potential energy of the system contributed by normal spring elements and tangential spring elements, respectively, l is the distance between the location of the distributed springs to the x-y plane. Then through the Lagrange's approach, we have the equations of motion as

$$
\begin{aligned}
&M\ddot{u}+\{2k_nl_L\cos^2\beta+2k_sl_L\sin^2\beta\}u\\
&+\{-2k_nl_Ld\cos^2\beta-2k_nl_Le\sin\beta\cos\beta-2k_sl_Ld\sin^2\beta+2k_sl_Le\sin\beta\cos\beta\}\phi=0
\end{aligned} \tag{15}
$$

$$
M\ddot{v}+\{2k_nl_L\sin^2\beta+2k_sl_L\cos^2\beta\}v = 0 \tag{16}
$$

$$
\begin{aligned}
J_x\ddot{\phi}&+\{-2k_nl_Ld\cos^2\beta-2k_nl_Le\sin\beta\cos\beta-2k_sl_Ld\sin^2\beta+2k_nl_Le\sin\beta\cos\beta\}u\\
&+\{2k_nl_Ld^2\cos^2\beta+4k_nl_Lde\sin\beta\cos\beta+2k_nl_Le^2\sin^2\beta\}\phi\\
&+\{2k_sl_Ld^2\sin^2\beta-4k_sl_Lde\sin\beta\cos\beta+2k_sl_Le^2\cos^2\beta\}\phi=0
\end{aligned} \tag{17}
$$

$$
J_y\ddot{\theta}+\left\{\frac{k_n}{6}l_L^3\sin^2\beta+\frac{k_s}{6}l_L^3\cos^2\beta\right\}\theta = 0 \tag{18}
$$

$$
J_z\ddot{\psi}+\left\{\frac{k_n}{6}l_L^3\cos^2\beta+\frac{k_s}{6}l_L^3\sin^2\beta\right\}\psi = 0 \tag{19}
$$

From Eq. (16) of the displacement v along the z-axis, (18) of the angular displacement θ about y-axis and (19) of the angular displacement ψ about z-axis, the frequencies can be obtained as follows:
The natural frequency of the carriage at vertical vibration mode is

$$
f_V = \frac{1}{\pi}\sqrt{\frac{k_nl_L\sin^2\beta+k_sl_L\cos^2\beta}{2M}} \tag{20}
$$

The natural frequency of the carriage at pitching vibration mode is

$$
f_P = \frac{1}{2\pi}\sqrt{\frac{k_nl_L^3\sin^2\beta+k_sl_L^3\cos^2\beta}{6J_y}} \tag{21}
$$

The natural frequency of the carriage at yawing vibration mode is

$$
f_Y = \frac{1}{2\pi}\sqrt{\frac{k_nl_L^3\cos^2\beta+k_sl_L^3\sin^2\beta}{6J_z}} \tag{22}
$$

Eq. (15) of the displacement u along the y-axis and (17) of the angular displacement φ about x-axis are coupled. We may assume the solutions of the form:

$$\left.\begin{aligned} u &= Ue^{j\omega t} \\ \phi &= \Phi e^{j\omega t} \end{aligned}\right\} \tag{23}$$

where ω is the angular frequency, $j = \sqrt{-1}$, U and Φ are the amplitude of u and ϕ, respectively. Substituting Eq. (23) into Eqs. (15) and (17), yielding

$$\begin{bmatrix} c_1 - M\omega^2 & c_2 \\ c_2 & c_3 - J_x\omega^2 \end{bmatrix} \begin{bmatrix} U \\ \Phi \end{bmatrix} = 0 \tag{24}$$

where

$$\left.\begin{aligned} c_1 &= 2k_n l_L \cos^2\beta + 2k_s l_L \sin^2\beta \\ c_2 &= -2k_n d\cos^2\beta - 2k_n e\sin\beta\cos\beta - 2k_s l_L d\sin^2\beta + 2k_s l_L e\sin\beta\cos\beta \\ c_3 &= 2k_n l_L d^2\cos^2\beta + 4k_n l_L de\sin\beta\cos\beta + 2k_n l_L e^2\sin^2\beta \\ &\quad + 2k_s l_L d^2\sin^2\beta - 4k_s l_L de\sin\beta\cos\beta + 2k_s l_L e^2\cos^2\beta \end{aligned}\right\} \tag{25}$$

Let the determinant of the coefficient of U and Φ be zero, we have the characteristic equation.

$$MJ_x\omega^4 - (c_3M + c_1J_x)\omega^2 + c_1c_3 - c_2^2 = 0 \tag{26}$$

The two solutions ω_1^2 and $\omega_2^2(\omega_1^2 < \omega_2^2)$ can be obtained by solving above equation.

$$\omega_{1,2}^2 = \frac{c_3M + c_1J_x \mp \sqrt{(c_3M + c_1J_x)^2 - 4MJ_x(c_1c_3 - c_2^2)}}{2MJ_x} \tag{27}$$

The natural frequency of the carriage at different vibration mode can be written as the following Eqs. (28) and (29).
The natural frequency of the carriage at lower rolling vibration mode is

$$f_{RL} = \frac{\omega_1}{2\pi} \tag{28}$$

The natural frequency of the carriage at higher rolling vibration mode is

$$f_{RH} = \frac{\omega_2}{2\pi} \tag{29}$$

3.3 Moment effect on the natural frequency of the rigid-body carriage

Moments are usually generated by non-uniform loads distributed on the carriage. Under this loading condition, the rolling balls at both sides of raceway will experience different extent of contact loading, which in turn induces different normal stiffness k_n and tangential stiffness k_S at the rolling interface and hence affect the vibration characteristic of the guideway. To consider the moment effect on the natural frequency of the rigid-body carriage, we therefore derive the equilibrium equation for the carriage subjected to moment loading M_X, which is applied on carriage block along x-axis direction, and the kinetic energy E_K can be expressed as:

$$E_K = \frac{1}{2}M\dot{u}^2 + \frac{1}{2}M\dot{v}^2 + \frac{1}{2}J_x\dot{\phi}^2 + \frac{1}{2}J_y\dot{\theta}^2 + \frac{1}{2}J_z\dot{\psi}^2 \tag{30}$$

And, the potential energy E_p can be given by

$$E_P = E_{P1} + E_{P2} \tag{31}$$

$$\begin{aligned} E_{P1} = {} & \frac{1}{2}k_{n1}\int_0^{l_L/2}[\{(u - d\phi + l\psi)\cos\beta + (-v - e\phi + l\theta)\sin\beta\}^2 \\ & + \{(u - d\phi - l\psi)\cos\beta + (-v - e\phi - l\theta)\sin\beta\}^2]dl \\ & + \frac{1}{2}k_{n2}\int_0^{l_L/2}[\{(-u + d\phi - l\psi)\cos\beta + (-v + e\phi + l\theta)\sin\beta\}^2 \\ & + \{(-u + d\phi + l\psi)\cos\beta + (-v + e\phi - l\theta)\sin\beta\}^2]dl \end{aligned} \tag{32}$$

$$\begin{aligned} E_{P2} = {} & \frac{1}{2}k_{s1}\int_0^{l_L/2}[\{(u - d\phi + l\psi)\sin\beta + (v + e\phi - l\theta)\cos\beta\}^2 \\ & + \{(u - d\phi - l\psi)\sin\beta + (v + e\phi + l\theta)\cos\beta\}^2]dl \\ & + \frac{1}{2}k_{s1}\int_0^{l_L/2}[\{(u - d\phi + l\psi)\sin\beta + (-v + e\phi + l\theta)\cos\beta\}^2 \\ & + \{(u - d\phi - l\psi)\sin\beta + (-v + e\phi - l\theta)\cos\beta\}^2]dl \end{aligned} \tag{33}$$

where E_{P1} is potential energy stored in the left and right spring elements with normal stiffness k_{n1} and k_{n2}, E_{P2} is potential energy stored in the left and right spring elements with tangential stiffness k_{s1} and k_{s2}, and l is the distance between the location of the distributed spring and the x-y plane. The following five motion equations can therefore be obtained by applying the Lagrange's approach to Eqs. (30) and (31), that is

$$\begin{aligned} J_y\ddot{\theta} & + \left\{\frac{k_{n1}}{12}l_L^3\sin^2\beta + \frac{k_{n2}}{12}l_L^3\sin^2\beta + \frac{k_{s1}}{12}l_L^3\cos^2\beta + \frac{k_{s2}}{12}l_L^3\cos^2\beta\right\}\theta \\ & + \left\{\frac{k_{n1}}{12}l_L^3\sin\beta\cos\beta - \frac{k_{n2}}{12}l_L^3\sin\beta\cos\beta\right\}\psi \\ & + \left\{-\frac{k_{s1}}{12}l_L^3\sin\beta\cos\beta + \frac{k_{s2}}{12}l_L^3\sin\beta\cos\beta\right\}\psi = 0 \end{aligned} \tag{34}$$

$$J_z\ddot{\psi} + \left\{\frac{k_{n1}}{12}l_L^3\cos^2\beta + \frac{k_{n2}}{12}l_L^3\cos^2\beta + \frac{k_{s1}}{12}l_L^3\sin^2\beta + \frac{k_{s2}}{12}l_L^3\sin^2\beta\right\}\psi$$

$$+\left\{\frac{k_{n1}}{12}l_L^3\sin\beta\cos\beta-\frac{k_{n2}}{12}l_L^3\sin\beta\cos\beta\right\}\theta$$

$$+\left\{-\frac{k_{s1}}{12}l_L^3\sin\beta\cos\beta+\frac{k_{s2}}{12}l_L^3\sin\beta\cos\beta\right\}\theta=0 \tag{35}$$

$$\begin{aligned}M\ddot{u}&+\{k_{n1}l_L\cos^2\beta+k_{n2}l_L\cos^2\beta+k_{s1}l_L\sin^2\beta+k_{s2}l_L\sin^2\beta\}u\\&+\{-k_{n1}l_L\sin\beta\cos\beta+k_{n2}l_L\sin\beta\cos\beta+k_{s1}l_L\sin\beta\cos\beta-k_{s2}l_L\sin\beta\cos\beta\}v\\&+\{-k_{n1}l_Le\sin\beta\cos\beta-k_{n2}l_Le\sin\beta\cos\beta+k_{s1}l_Le\sin\beta\cos\beta+k_{s2}l_Le\sin\beta\cos\beta\}\phi\\&+\{-k_{n1}l_Ld\cos^2\beta-k_{n2}l_Ld\cos^2\beta-k_{s1}l_Ld\sin^2\beta-k_{s2}l_Ld\sin^2\beta\}\phi=0\end{aligned} \tag{36}$$

$$\begin{aligned}M\ddot{v}&+\{k_{n1}l_L\sin^2\beta+k_{n2}l_L\sin^2\beta+k_{s1}l_L\cos^2\beta+k_{s2}l_L\cos^2\beta\}v\\&+\{-k_{n1}l_L\sin\beta\cos\beta+k_{n2}l_L\sin\beta\cos\beta+k_{s1}l_L\sin\beta\cos\beta-k_{s2}l_L\sin\beta\cos\beta\}u\\&+\{k_{n1}l_Ld\sin\beta\cos\beta-k_{n2}l_Ld\sin\beta\cos\beta-k_{s1}l_Ld\sin\beta\cos\beta+k_{s2}l_Ld\sin\beta\cos\beta\}\phi\\&+\{k_{n1}l_Le\sin^2\beta-k_{n2}l_Le\sin^2\beta+k_{s1}l_Le\cos^2\beta-k_{s2}l_Le\cos^2\beta\}\phi=0\end{aligned} \tag{37}$$

$$\begin{aligned}J_x\ddot{\phi}&+\{k_{n1}l_Ld^2\cos^2\beta+2k_{n1}l_Lde\sin\beta\cos\beta+k_{n1}l_Le^2\sin^2\beta\}\phi\\&+\{k_{n2}l_Ld^2\cos^2\beta+2k_{n2}l_Lde\sin\beta\cos\beta+k_{n2}l_Le^2\sin^2\beta\}\phi\\&+\{k_{s1}l_Ld^2\sin^2\beta-2k_{s1}l_Lde\sin\beta\cos\beta+k_{s1}l_Le^2\cos^2\beta\}\phi\\&+\{k_{s2}l_Ld^2\sin^2\beta-2k_{s2}l_Lde\sin\beta\cos\beta+k_{s2}l_Le^2\cos^2\beta\}\phi\\&+\{-k_{n1}l_Le\sin\beta\cos\beta-k_{n2}l_Le\sin\beta\cos\beta+k_{s1}l_Le\sin\beta\cos\beta+k_{s2}l_Le\sin\beta\cos\beta\}u\\&+\{-k_{n1}l_Ld\cos^2\beta-k_{n2}l_Ld\cos^2\beta-k_{s1}l_Ld\sin^2\beta-k_{s2}l_Ld\sin^2\beta\}u\\&+\{k_{n1}l_Ld\sin\beta\cos\beta-k_{n2}l_Ld\sin\beta\cos\beta-k_{s1}l_Ld\sin\beta\cos\beta+k_{s2}l_Ld\sin\beta\cos\beta\}v\\&+\{k_{n1}l_Le\sin^2\beta-k_{n2}l_Le\sin^2\beta+k_{s1}l_Le\cos^2\beta-k_{s2}l_Le\cos^2\beta\}v=0\end{aligned} \tag{38}$$

Eqs. (34) and (35) show the angular displacements θ about the y-axis and ψ about the z-axis are coupled. To discuss the two interrelated variables, the variables in Eqs. (34) and (35) are assumed as:

$$\left.\begin{aligned}\theta&=\Theta e^{j\omega t}\\\psi&=\Psi e^{j\omega t}\end{aligned}\right\} \tag{39}$$

where ω is angular velocity, $j=\sqrt{-1}$, Θ and Ψ represent the amplitude of θ and ψ, respectively. Substituting Eq. (39) into Eqs. (34) and (35), the following equation can be obtained

$$\begin{bmatrix}c_1-J_Y\omega^2 & c_2\\ c_2 & c_3-J_Z\omega^2\end{bmatrix}\begin{bmatrix}\Theta\\\Psi\end{bmatrix}=0 \tag{40}$$

Where

$$\left.\begin{aligned} c_1 &= \frac{k_{n1}}{12} l_L^3 \sin^2\beta + \frac{k_{n2}}{12} l_L^3 \sin^2\beta + \frac{k_{s1}}{12} l_L^3 \cos^2\beta + \frac{k_{s2}}{12} l_L^3 \cos^2\beta \\ c_2 &= \frac{k_{n1}}{12} l_L^3 \sin\beta\cos\beta - \frac{k_{n2}}{12} l_L^3 \sin\beta\cos\beta - \frac{k_{s1}}{12} l_L^3 \sin\beta\cos\beta + \frac{k_{n2}}{12} l_L^3 \sin\beta\cos\beta \\ c_3 &= \frac{k_{n1}}{12} l_L^3 \cos^2\beta + \frac{k_{n2}}{12} l_L^3 \cos^2\beta + \frac{k_{s1}}{12} l_L^3 \sin^2\beta + \frac{k_{s2}}{12} l_L^3 \sin^2\beta \end{aligned}\right\} \quad (41)$$

The characteristic equation can be obtained by letting the determinant of factors Θ and Ψ be zero, that is

$$J_y J_z \omega^4 - (c_3 J_y + c_1 J_z)\omega^2 + c_1 c_3 - c_2^2 = 0 \quad (42)$$

At last, two solutions ω_1^2 and $\omega_2^2(\omega_1^2 < \omega_2^2)$ are derived

$$\omega_{1,2}^2 = \frac{c_3 J_y + c_1 J_z \mp \sqrt{(c_3 J_y + c_1 J_z)^2 - 4 J_y J_z (c_1 c_3 - c_2^2)}}{2 J_y J_z} \quad (43)$$

Since this coupled vibration is contributed by the displacement components Θ and Ψ, the vibration mode is therefore called the yawing-pitching vibration mode the carriage. Again, the smaller value of ω is associated with lower yawing-pitching vibration mode, and the other is associated with higher yawing-pitching vibration mode. The natural frequency of the carriage at different vibration mode can be found in the following Eqs. (44) and (45).

The natural frequency of the carriage at lower yawing-pitching mode is

$$f_{YPL} = \frac{\omega_1}{2\pi} \quad (44)$$

The natural frequency of the carriage at higher yawing-pitching mode is

$$f_{YPH} = \frac{\omega_2}{2\pi} \quad (45)$$

Similarly, Eqs. (36), (37) and (38) show the displacements u, v along y-axis, z-axis and the angular displacement ϕ about the z-axis are coupled. Therefore, in order to discuss three interrelated variables, the solution of Eqs. (36), (37) and (38) are assumed as:

$$\left.\begin{aligned} u &= U e^{j\omega t} \\ v &= V e^{j\omega t} \\ \phi &= \Phi e^{j\omega t} \end{aligned}\right\} \quad (46)$$

where, ω is angular velocity, $j = \sqrt{-1}$. U, V and Φ represent the amplitude of u, v and ϕ, respectively.

Substituting Eq. (46) into (36), (37) and (38), the following equation can be obtained

$$\begin{bmatrix} c_4 - M\omega^2 & c_5 & c_7 \\ c_5 & c_6 - M\omega^2 & c_8 \\ c_7 & c_8 & c_9 - J_x\omega^2 \end{bmatrix} \begin{bmatrix} U \\ V \\ \Phi \end{bmatrix} = 0 \tag{47}$$

Where

$$\left.\begin{aligned} c_4 &= k_{n1}l_L\cos^2\beta + k_{n2}l_L\cos^2\beta + k_{s1}l_L\sin^2\beta + k_{s2}l_L\sin^2\beta \\ c_5 &= -k_{n1}l_L\sin\beta\cos\beta + k_{n2}l_L\sin\beta\cos\beta + k_{s1}l_L\sin\beta\cos\beta - k_{s2}l_L\sin\beta\cos\beta \\ c_6 &= k_{n1}l_L\sin^2\beta + k_{n2}l_L\sin^2\beta + k_{s1}l_L\cos^2\beta + k_{s2}l_L\cos^2\beta \\ c_7 &= -k_{n1}l_Le\sin\beta\cos\beta - k_{n2}l_Le\sin\beta\cos\beta + k_{s1}l_Le\sin\beta\cos\beta + k_{s2}l_Le\sin\beta\cos\beta \\ &\quad -k_{n1}l_Ld\cos^2\beta - k_{n2}l_Ld\cos^2\beta - k_{s1}l_Ld\sin^2\beta - k_{s2}l_Ld\sin^2\beta \\ c_8 &= k_{n1}l_Ld^2\cos^2\beta + 2k_{n1}l_Lde\sin\beta\cos\beta + k_{n1}l_Le^2\sin^2\beta \\ &\quad + k_{n2}l_Ld^2\cos^2\beta + 2k_{n2}l_Lde\sin\beta\cos\beta + k_{n2}l_Le^2\sin^2\beta \\ &\quad + k_{s1}l_Ld^2\sin^2\beta - 2k_{s1}l_Lde\sin\beta\cos\beta + k_{s1}l_Le^2\cos^2\beta \\ &\quad + k_{s2}l_Ld^2\sin^2\beta - 2k_{s2}l_Lde\sin\beta\cos\beta + k_{s2}l_Le^2\cos^2\beta \\ c_9 &= k_{n1}l_Ld\sin\beta\cos\beta - k_{n2}l_Ld\sin\beta\cos\beta - k_{s1}l_Ld\sin\beta\cos\beta + k_{s2}l_Ld\sin\beta\cos\beta \\ &\quad + k_{n1}l_Le\sin^2\beta - k_{n2}l_Le\sin^2\beta + k_{s1}l_Le\cos^2\beta - k_{s2}l_Le\cos^2\beta \end{aligned}\right\} \tag{48}$$

Again, the characteristic equation can be obtained by making the determinant of factors U, V and Φ be zero which yields.

$$\omega^6 + a_1\omega^4 + a_2\omega^2 + a_3 = 0 \tag{49}$$

$$\left.\begin{aligned} a_1 &= -\left(\frac{c_4MJ_x + c_6MJ_x + c_8M^2}{M^2J_x}\right) \\ a_2 &= -\left(\frac{c_7^2M + c_9^2M + c_5^2J_x - c_6c_8M - c_4c_8M - c_4c_6J_x}{M^2J_x}\right) \\ a_3 &= -\left(\frac{c_4c_6c_8 + 2c_5c_7c_9 - c_7^2c_6 - c_9^2c_4 - c_5^2c_8}{M^2J_x}\right) \end{aligned}\right\} \tag{50}$$

Finally, three solutions ω_3^2, ω_4^2 and $\omega_5^2 (\omega_3^2 < \omega_4^2 < \omega_5^2)$ are obtained

$$\left.\begin{aligned} \omega_3 &= \left\{2\sqrt{-Q}\cos\left(\frac{1}{3}\gamma\right) - \frac{1}{3}a_1\right\}^{\frac{1}{2}} \\ \omega_4 &= \left\{2\sqrt{-Q}\cos\left(\frac{1}{3}\gamma + 120^{\circ}\right) - \frac{1}{3}a_1\right\}^{\frac{1}{2}} \\ \omega_5 &= \left\{2\sqrt{-Q}\cos\left(\frac{1}{3}\gamma + 240^{\circ}\right) - \frac{1}{3}a_1\right\}^{\frac{1}{2}} \end{aligned}\right\} \tag{51}$$

where

$$\left.\begin{aligned} Q &= \frac{3a_2 - a_1^2}{9} \\ R &= \frac{9a_1a_2 - 27a_3 - 2a_1^3}{54} \\ \cos\gamma &= \frac{R}{\sqrt{-Q^3}} \end{aligned}\right\} \tag{52}$$

The natural frequencies corresponding to various rolling vibration modes can then be obtained from Eq. (51) as shown in following Eqs. (53), (54) and (55).
The natural frequency of the carriage at lower rolling mode is

$$f_{RL} = \frac{\omega_3}{2\pi} \tag{53}$$

The natural frequency of the carriage at medium rolling mode is

Table 1 Specifications of the linear guide system

Carriage length	0.0659 m
Carriage width	0.059 m
Carriage height	0.022 m
Guideway length	0.5 m
Guideway width	0.02 m
Guideway height	0.0155 m
Ball diameter	4.763×10^{-3} m
Total number of balls	50
Number of row	2
Contact angle β	45°
Preload	665 N
Load zone length l_L	0.043 m

Table 2 Constants of the linear guide system

M	0.313 kg
J_x	9.938×10^{-5} kg-m^2
J_y	6.136×10^{-5} kg-m^2
J_z	1.394×10^{-4} kg-m^2
d	7.37×10^{-3} m
e	10.3×10^{-3} m
k_n	2.28 GPa
k_s	0.228 GPa

Table 3 Normal stiffness k_n and tangential stiffness k_s of a linear guideway

M_X (N-m)	Left row		Right row	
	k_n (GPa)	k_s (GPa)	k_n (GPa)	k_s (GPa)
0	2.28	0.228	2.28	0.228
2.38	2.17	0.217	2.38	0.238
4.75	2.04	0.204	2.48	0.248
7.13	1.89	0.189	2.57	0.257

$$f_{RM} = \frac{\omega_4}{2\pi} \tag{54}$$

The higher rolling frequency of the vibration of the carriage is

$$f_{RH} = \frac{\omega_5}{2\pi} \tag{55}$$

The detailed specifications of linear guide system are listed in Table 1. With introduction of constants β, l_L in Table 1 and constants M, J_x, J_y, J_z, d, e, k_n, k_s in Tables 2 and 3 into the equation of section 3.2 we can then calculate the natural frequencies f_{RL}, f_{YPL}, f_{YPH}, f_{RM} and f_{RH} of carriage block under different M_X (x-axis force moment).

4. The finite element approach

Fig. 6 shows the 3-D finite element model of a linear guideway mechanism. The contact configuration between balls and raceway and carriage is depicted in Fig. 7, in which the two rows of the rolling balls are modeled with brick elements (Fig. 8). To model the contact characteristic at the rolling interface, the contact elements of zero thickness are introduced at upper and lower side of each ball. There are two rows, 18 balls located within the loading zone, which were meshed into 144 elements and 36 contact interface elements. The carriage block and end cap at both sides were meshed with 3830 elements and 480 elements, respectively, while the base of the guideway was modeled using 2158 elements. There are totally 6648 elements and 9396 nodes. The main components such as ball, carriage and guideway are made of steel with the material properties: Young's modulus E = 206 GPa, Poisson's ratio ν = 0.305, density ρ = 7800 Kg/m^3, while the end caps have the properties: E = 206 GPa, Poisson ratio $\nu = 0.305$, density $\rho = 1400$ Kg/m^3.

Besides, the stiffnesses k_n and k_s of the contact element were calculated according to the method described in section 2.1. The stiffness K_C was assigned between the carriage block and ball bearing, and the stiffness K_R was between steel balls and guideway. The same properties were assumed for all contact interfaces as $K_C = K_R = K_n$.

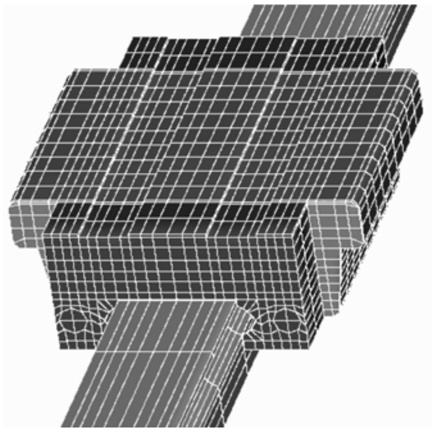

Fig. 6 The finite element model of a linear guide system, including guideway, carriage, rolling balls and end cap

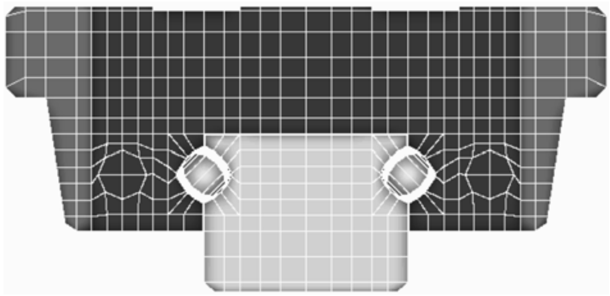

Fig. 7 Finite element mesh of transverse cross section, showing the contact configuration between carriage and guideway

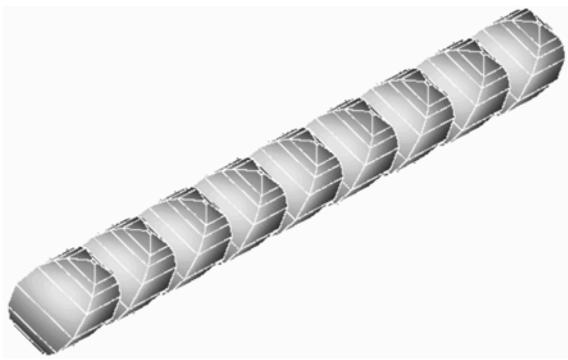

Fig. 8 Simulation of the steel balls row by row

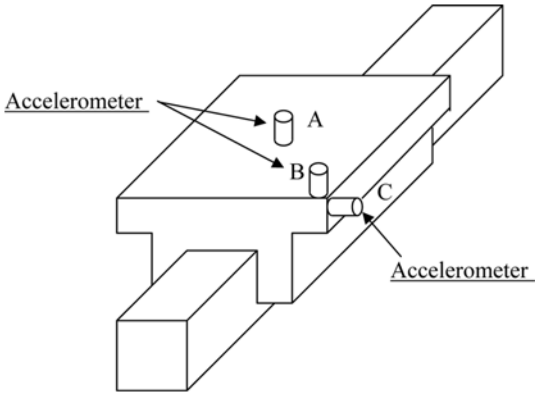

Fig. 9 Configuration of modal experiment and accelerometer positions (A, B, C) for measuring various vibration mode

5. The experiment verification

To understand the significance of current methods, modal tests on workshop supplied guideways were conducted in this study. Fig. 9 shows the experimental configuration for measuring the vibration of the linear guide system. The accelerometer was attached to different position on the carriage, in which the accelerometer A was used to measure the vertical vibration of carriage, accelerometer B mainly was for rolling, pitching vibrations and vertical vibration and accelerometer

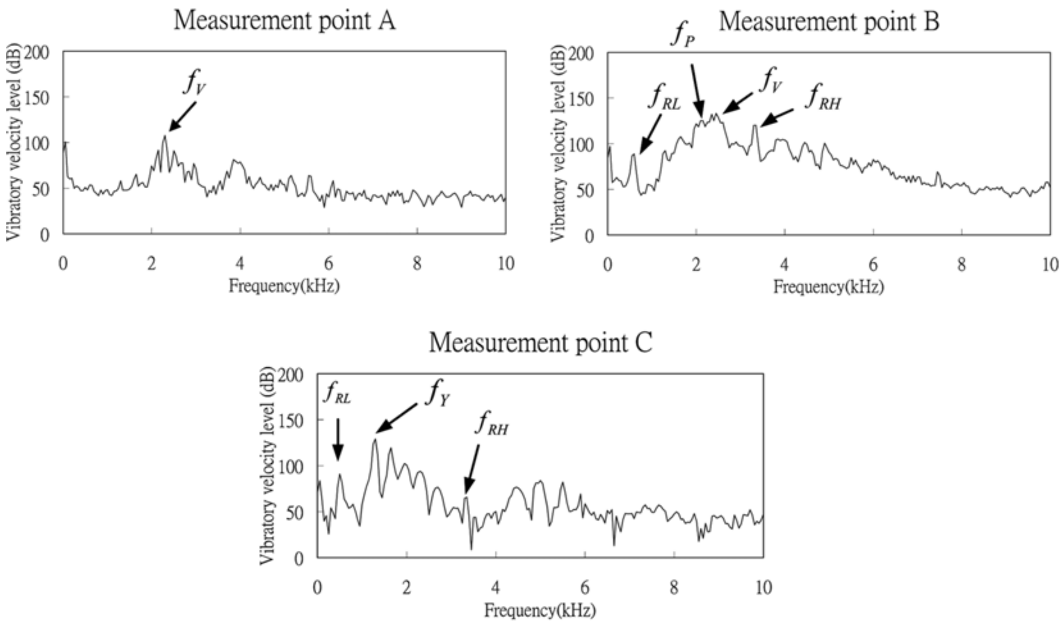

Fig. 10 Vibration spectra measured at different positions, representing the possible vibration modes of a carriage, respectively

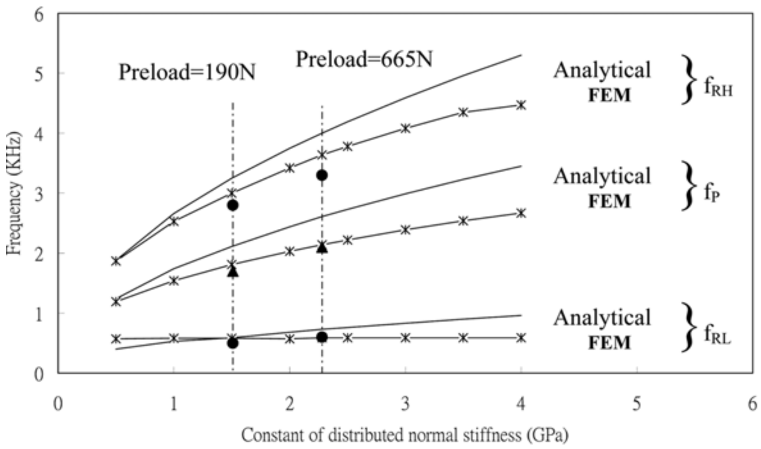

(a) Lower rolling, pitching and higher rolling mode

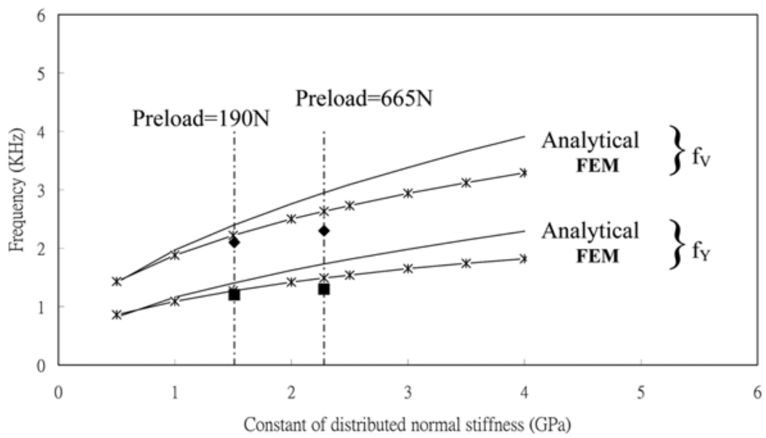

(b) Yawing and vertical mode

Fig. 11 Comparison of the natural frequencies obtained from experimental measurements, analytical and finite element prediction. Bold symbols in figure represent the experimental data at different mode, respectively.

C was for yawing and rolling vibrations. For investigation of the effect of the contact stiffness in the dynamic behaviors, two linear guideways with different preload, one for high preload of 665 N and low preload of 190 N, for another, were employed during test. In experiment, the vibration amplitudes were recorded and stored in a digital spectrum analyzer after hammering the carriage at the measured direction.

From above measurements, the vibration spectra corresponding to the three measuring points A, B and C were depicted in Fig. 10. The main peaks of each measurement point to obtain the fundamental frequency were generalized, and the associated vibration modes can be identified by comparing to the mode shapes predicted by the finite element approach (Table 4). Experimental results are depicted in Fig. 11 comparing with the numerical results obtained from theoretical and finite element analysis.

Table 4 Natural frequencies at different vibration mode of a linear guide system

(a) Analytical approach : 2-D point-to-point elastic contact

$M_X = 0$			$M_X = 4.75$ N-m		
Degree of freedom	mode	Frequency (kHz)	Degree of freedom	mode	Frequency (kHz)
ϕ, u	Lower rolling	0.73(f_{RL})	ϕ, u, v	Lower rolling	0.72(f_{RL})
ψ	Yawing	1.73(f_Y)	ψ, θ	Lower Yawing-Pitching	1.71(f_{YPL})
θ	Pitching	2.61(f_P)	θ, ψ	Higher Yawing-Pitching	2.60(f_{YPH})
v	Vertical	2.95(f_V)	v, u, ϕ	Medium rolling	2.90(f_{RM})
ϕ, u	Higher rolling	4.00(f_{RH})	ϕ, u, v	Higher rolling	4.00(f_{RH})

(b) Finite element approach

$M_X = 0$			$M_X = 4.75$ N-m		
Degree of freedom	mode	Frequency (kHz)	Degree of freedom	mode	Frequency (kHz)
ϕ, u	Lower rolling	0.59(f_{RL})	ϕ, u, v	Lower rolling	0.59(f_{RL})
ψ	Yawing	1.49(f_Y)	ψ, θ	Lower Yawing-Pitching	1.48(f_{YPL})
θ	Pitching	2.14(f_P)	θ, ψ	Higher Yawing-Pitching	2.14(f_{YPH})
v	Vertical	2.63(f_V)	v, u, ϕ	Medium rolling	2.62(f_{RM})
ϕ, u	Higher rolling	3.64(f_{RH})	ϕ, u, v	Higher rolling	3.63(f_{RH})

6. Results and discussion

The natural frequencies of carriage block estimated by proposed analytical method and finite element approach are listed in Table 4. It can be found that both approaches predicted the same vibration modes. It is worthy to note that all the components of linear guideway mechanism are assumed to be rigid in the analytical method. Therefore, the analytical method may give higher frequencies than those obtained by the finite element approach (Table 4).

To study the effect of the loading conditions on the vibration mode, some specific modes are listed in Table 4. It is found that when the carriage block is without moment loadings, it will vibrate with natural frequency f_{RL}, f_Y, f_P, f_V and f_{RH} (see before). However, if a moment loading Mx is applied to the carriage block, it will vibrate at frequency f_{RL}, f_{YPL}, f_{YPH}, f_{RM} and f_{RH}. As observed in Table 4, the carriage block behaves different mode shapes under the absence of moment or in the event of presence of moments. In the second and the third modes, for example, when carriage block is not subjected to external moments, the natural frequencies f_Y and f_P of carriage block are only related to the variable ψ rotating around z-axis and variable θ rotating around y-axis, respectively. In case where carriage block subjects to external moments, the natural frequencies f_{YPL} and f_{YPH} of the carriage block are related to both displacement components of ψ and θ. Besides, when carriage block in fourth mode is not subjected to moment, the natural frequency f_V of carriage block is only related to variable v shifting along z-axis. While under moment loadings, the natural frequency f_{RM} of carriage block is related to displacement components u shifting along y-axis, ϕ rolling about x-axis and v shifting along z-axis.

On the other hand, results listed in Table 4 indicate that the 2-D point-to-point contact model may predict higher frequencies than the finite element method. This can be ascribed to that the guideway is assumed as an elastic material in the finite element approach and hence possess a lower structural stiffness than a rigid one in the analytical method. Actually, it can be realized from Hertz's contact theory that the material stiffness plays an important role on contact stiffness at the rolling interface. For carriage with sufficiently higher Young's modulus, it will behave as rigid body and give vibrational behaviors with higher frequencies. In addition, the guideway system discussed in this study is designed with the offset Gothic arc groove, which enables the rolling ball to contact with carriage and raceway simultaneously, and hence only two rolling interfaces are formed. One is between the rolling ball and the groove of carriage and another is between the rolling ball and the groove of rail. The interface elements with normal and tangential stiffness are thus introduced at upper and lower interfaces of the rolling ball in the finite element model. In the late of 2005, a new production with heavy-duty guideway has been designed in workshop with symmetric Gothic arc grooves to sustain a great deal of axial and radial force, which gives a four-point contact configuration at various contact angles. Under such condition, the simulation of contact characteristic at the rolling interface also can be achieved by introducing the interface element at the four contact points. The contact stiffness at each interface can be calculated according to the contact configuration formed within the guideway. Besides, preload on the rolling element also plays an important role in either improvement of the rigidity or accuracy of a guideway (NSK Ltd.). However preload also initiates another problem such as significant friction and contact deformation at the raceway groove. It follows that bring the initial contact stiffness of the rolling ball to a different value. The influence of preload on the dynamic characteristic of a linear guideway is investigated through modal experiments.

As a validation, a series of model tests have been conducted on guideway mechanisms. It is apparent from Fig. 10 that the experimental results agree well with the finite element prediction, but have a little bit lower than the analytical results. As stated in previous sections, the linear guideway is modeled as an elastic structure in the finite element approach, rather than a rigid one assumed in analytical method; therefore, the finite element approach may present like a real guideway mechanism than the analytical method. In addition, results of modal tests indicate that a guideway with high preload has a higher vibration frequency than that with low preload. It illustrates that different extents of preload set in guideway induce a change of contact stiffness at rolling interface and hence results in the variation in vibration frequencies. Especially, such an effect can be demonstrated by the finite element simulation.

In summary, the 3-D surface-to-surface finite element model offers better results than 2-D point-to-point contact model. In addition, some differences in simulation of the contact mode of a guideway also can be emphased. In analytical method, the contact configuration between balls and raceway groove of carriage and guideway is considered as a point-to-point contact mode and the rolling balls are simulated by a series of spring elements connecting the carriage and guide rail along the direction of contact angle. While in the finite element approach, the rolling interfaces between balls and raceway groove of carriage and guideway are considered as a surface-to-surface contact mode. The contact stiffness at each interface is simulated by interface elements introduced on the top and bottom surface of the rolling balls. In addition, the effect of the stiffness of a rolling ball can be raised in finite element approach, whereas this effect was not considered in the analytical method. However, comparison of the results obtained from experiment and numerical prediction have told the distinctiveness of the finite element approach. In a word, the presented finite element method based on Hertz's contact theory can accurately describe the contact characteristic of a rolling interface and provide a reliable way to investigate the dynamic characteristic of a linear guidway mechanism.

7. Conclusions

The following conclusions are drawn from analytical method, the finite element approach and experiment of modal tests.

1. The dynamic behavior of linear guide system has been shown to be closely related to the structure stiffness, especially, the contact stiffness at the rolling interface between the steel balls and the Gothic groove of the carriage and guideway. While the contact stiffness can be accurately obtained based on the Hertz's contact theory, which can further be used to model the contact characteristic under different loading conditions.
2. The introduction of the contact element with Hertzian contact stiffness can predict the influence of loading condition on the dynamic characteristic such as natural frequencies and modal shapes in more realistic issues.
3. In this paper, the proposed finite element method has shown that the vibration behaviors of a linear guideway can be characterized (a) with the lower rolling natural frequency of the vibration, (b) with the lower yawing-pitching natural frequency of the vibration, (c) with the higher yawing-pitching natural frequency of the vibration, (d) with the medium rolling natural frequency of the vibration, and (e) with the higher rolling natural frequency of the vibration.

References

Egert, J. (2000), "Comparison of some contact elements and iterative algorithms for the solution of frictionless contact problems", *J. Comput. Appl. Mech.*, **1**(1), 23-36.

Goldsmith, W. (1960), *Impact-the Theory and Physical Behavior of Colliding Solids*, Edward Arnold Ltd.

Hernot, X., Sartor, M. and Guillot, J. (2000), "Calculation of the stiffness matrix of angular contact ball bearings by using the analytical approach", *J. Mech. Design*, **122**(March), 83-90.

Hwang, D.H. and Gahr, K.H. (2003), "Transition from static to kinetic friction of unlubricated or oil lubricated steel/steel, steel/ceramic and ceramic/ceramic pairs", *Wear*, **255**, 365-375.

Johnson, K.J. (1985), *Contact Mechanics*, Cambridge University Press.

Lynagh, N., Rahnejat, H., Erahimi, M. and Aini, R. (2000), "Bearing induced vibration in precision high speed routing spindle", *Int. J. Machine Tools & Manufacture*, **40**, 561-577.

NSK Corporation Ltd., "A-II technical description of NSK linear guides", *Selection Guide to NSK Linear Guides.*

Ohta, H. (1999), "Sound of guideway type recirculating linear ball bearings", *Transactions of the ASME Journal of Tribology*, **121**, 678-685.

Ohta, H. and Hayashi, E. (2000), "Vibration of linear guideway type recirculating linear ball bearings", *J. Sound Vib.*, **235**(5), 847-861.

Pimsarn, M. and Kazerounian, K. (2002), "Efficient evaluation of spur gear tooth mesh load using pseudo-interference stiffness estimation method", *Mechanism and Machine Theory*, **37**, 769-786.